AIAA JOURNAL
Vol. 40, No. 9, September 2002

Detachment of the Dynamic-Stall Vortex Above a Moving Surface

Aleksandr V. Obabko* and Kevin W. Cassel†
Illinois Institute of Technology, Chicago, Illinois 60616

Dynamic stall occurs on helicopter blades and pitching airfoils when the dynamic-stall vortex, which forms as a result of an unsteady boundary-layer eruption near the leading edge, detaches from the surface and convects into the wake of the airfoil. The dynamic-stall vortex is modeled as a thick-core vortex above an infinite plane surface. Numerical solutions of the unsteady Navier–Stokes equations are obtained to determine the nature of the unsteady separation and vortex detachment processes and the influence of a moving wall. Whereas the unsteady separation process evolves very differently within two Reynolds number regimes, the detachment process is observed to be very similar over the range of Reynolds numbers considered. A moving wall has a significant influence on both processes. It is found that increasing the wall speed toward a critical value, which is equal to the magnitude of the maximum inviscid velocity at the surface, results in solutions that are indicative of flows at lower Reynolds numbers. Eventually, for wall speeds close to this critical value, formation of the recirculation region and unsteady separation are suppressed altogether, and detachment of the vortex is prevented.

Nomenclature

a	=	streamwise grid transformation parameter
b	=	normal grid transformation parameter
k	=	thick-core vortex parameter
Re	=	Reynolds number
(r, θ)	=	cylindrical coordinates
r_0	=	normal distance to vortex center
t	=	time
$\|U_e\|_{\max}$	=	maximum magnitude of inviscid streamwise velocity at surface
U_0	=	freestream velocity in fixed frame of reference
(u, v)	=	streamwise and normal velocities
V_c	=	streamwise vortex convection velocity
(x, y)	=	streamwise and normal coordinates
$(\hat{x}, \hat{y})$	=	streamwise and normal computational coordinates
x_0	=	center of streamwise grid transformation
α	=	fractional convection rate of vortex
β	=	nondimensional wall speed
β_c	=	critical wall speed
β_m	=	$\|U_e\|_{\max}$
ν	=	kinematic viscosity
ψ	=	stream function
ψ_0	=	inviscid stream function
ω	=	vorticity

Subscript

s	=	unsteady boundary-layer singularity

Superscript

$*$	=	dimensional variables

I. Introduction

DYNAMIC stall at high Reynolds numbers involves a sequence of events that leads to the formation and subsequent detachment of a vortex above pitching airfoils, helicopter blades, and compressor blades.[1–3] As the angle of attack of an airfoil is increased, an increasingly adverse pressure gradient forms immediately downstream from the leading edge, which results in the formation of a recirculation region. At high Reynolds numbers Re, unsteady separation results in an eruptive boundary-layer response in which vorticity is ejected and ultimately rolls up to form the dynamic-stall vortex. For the period of time that the dynamic-stall vortex remains attached to the suction surface of the airfoil, there is an increase in lift. The presence of the vortex, however, induces a locally adverse streamwise pressure gradient that leads to a second unsteady boundary-layer eruption. A subsequent interaction involving the erupting spire, dynamic-stall vortex, and mainstream flow causes the vortex to detach from the surface and convect downstream. When the vortex convects past the trailing edge, the airfoil experiences a sudden loss of lift and a pitching moment. Dynamic stall is an interesting example of unsteady separation in which the adverse pressure gradients that initiate the eruptive processes are induced both by the geometry, that is, near the leading edge, and by the presence of a vortex.

A significant amount of effort has been devoted to increasing our understanding of dynamic stall through both experimental and numerical investigations.[4–11] The ultimate objectives of these efforts are to improve our physical understanding of unsteady separation and dynamic stall and to guide the development of techniques for controlling such events. In some applications, such as rotorcraft and turbomachinery, it is typically desired to suppress dynamic stall altogether to maintain smooth attached flow. In other applications, such as high-angle-of-attack aircraft, it may be possible to increase maneuverability by taking advantage of the high-lift stage of the dynamic-stall process.

A number of approaches have been considered for controlling unsteady separation and dynamic stall. For example, Chandrasekhara et al.[12] have demonstrated that the stall angle of an airfoil can be delayed using an adaptive airfoil leading edge that is capable of changing shape locally, thus altering the pressure distribution. It has been shown experimentally that leading-edge suction can be effective in controlling formation of the dynamic-stall vortex on airfoils by Karim and Acharya[13] and Alrefai and Acharya.[14] Cassel[15] considered the mixed convection induced by a rectilinear vortex above a heated surface at various angles of inclination and found that the onset of the boundary-layer eruption can be accelerated or delayed by the action of buoyancy forces on the heated near-wall fluid.

Solutions of the unsteady boundary-layer equations in regions of adverse pressure gradient inevitably result in formation of a singularity as the boundary layer grows rapidly toward a local eruption.[16,17] The influence of a moving wall on this process has been considered by Doligalski and Walker[18] and Degani et al.[19] Degani et al.

Presented as Paper 2001-2711 at the AIAA 31st Fluid Dynamics Conference, Anaheim, CA, 11–14 June 2001; received 15 July 2001; revision received 22 March 2002; accepted for publication 5 April 2002.

*Senior Research Associate, Mechanical, Materials and Aerospace Engineering Department. Member AIAA.
†Associate Professor, Mechanical, Materials and Aerospace Engineering Department. Member AIAA.

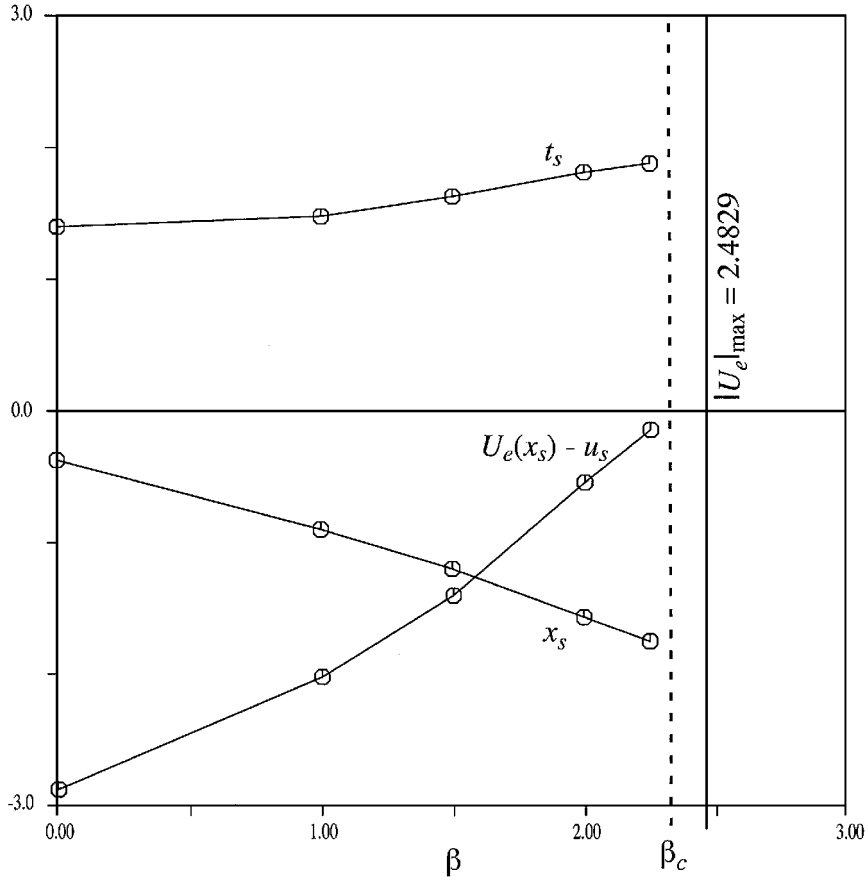

Fig. 1 Singularity time t_s, streamwise position x_s, and speed relative to the external velocity $U_e(x_s) - u_s$ from solutions of the unsteady boundary-layer equations for the thick-core vortex (from Cassel and Obabko[20]).

considered two model problems involving moving walls: the translating and rotating circular cylinder and a rectilinear vortex convected in a uniform flow above a moving wall. It was found that unsteady separation can be suppressed for wall speeds beyond a certain critical value. This critical wall speed β_c is slightly less than the maximum magnitude of the external velocity at the outer edge of the boundary layer due to the inviscid flow.

Similar calculations of the unsteady boundary-layer equations have been carried out for the thick-core vortex, which is considered in this investigation, by Cassel and Obabko.[20] The results corroborate the findings of Degani et al.[19] and are summarized in Fig 1. The nondimensional wall speed is β, and the maximum magnitude of the external velocity is $|U_e|_{\max} = 2.4829$. As β is increased from zero, the singularity time t_s is delayed ($t_s = 1.402$ for $\beta = 0$), and the streamwise position of the singularity x_s moves downstream toward the outflow stagnation point at $x = -2.0811$. Suppression of the singularity occurs at $\beta_c \approx 2.3$, when the difference between the local external velocity at the streamwise location of the separation point $U_e(x_s)$ and the streamwise speed of the separation point u_s goes to zero. Just as in Ref. 19, this critical wall speed is slightly less than the maximum magnitude of the external velocity $|U_e|_{\max}$.

In the present study, it is of interest to consider numerical solutions of the Navier–Stokes equations over a range of Reynolds numbers and wall speeds to determine how the moving wall mechanism differs as compared to the unsteady boundary-layer results, which apply as $Re \to \infty$. Cassel,[21] Obabko,[22] and Obabko and Cassel[23] considered the case of a thick-core vortex with $\beta = 0$ and found that, in terms of the spike formation process and viscous–inviscid interaction, there are three Reynolds number regimes. The high-Reynolds-number regime is characterized by solutions of the unsteady boundary-layer equations, which result in a very narrow eruption that leads to a small-scale interaction. In the moderate-Reynolds-number regime, the recirculation region forms just as in the boundary-layer case, followed by formation of the spike on the upstream side of the recirculation region; however, the spike formation process is accelerated due to a large-scale interaction that is insignificant in the high-Reynolds-number regime. In the low-Reynolds-number regime, the spike does not form; instead, the recirculation region continues its growth and interacts with the thick-core vortex.

The near-wall flow development is somewhat different in the low- and moderate-Reynolds-number regimes. In the moderate-Reynolds-number regime, the recirculation region induced by the adverse pressure gradient undergoes a series of eddy splittings due to the growth of secondary recirculation regions and ejections of near-wall vorticity, which produces a series of corotating eddies. These eddies later begin to merge one-by-one before moving away from the surface, which causes the thick-core vortex to detach. Results in the low-Reynolds-number regime do not exhibit this eddy splitting; rather, the primary recirculation region causes the thick-core vortex to detach in a manner similar to that of the merged eddies in the moderate-Reynolds-number regime.

It is found in this investigation that, in terms of the near-wall flow evolution, the moving wall effectively increases or decreases the Reynolds number depending on whether the wall moves in the same direction as the external flow, effectively decreasing the Reynolds number, or in the opposite direction, effectively increasing the Reynolds number. For example, a case that for $\beta = 0$ is in the moderate-Reynolds-number regime can be altered by increasing the wall speed to a flow that is representative of the low-Reynolds-number regime. In terms of vortex detachment, however, the process is delayed with increasing wall speed until a wall speed close to the maximum inviscid streamwise velocity $|U_e|_{\max}$ is reached, above which the recirculation region does not form and vortex detachment is suppressed. In other words, to prevent vortex detachment requires suppression of formation of the recirculation region (in a frame of reference moving with the vortex), not only suppression of spike formation and eruption. Note that these results may alternatively be viewed within the context of a convecting vortex above a stationary surface, where β becomes the nondimensional convection velocity of the vortex relative to the surface.

II. Formulation

A. Thick-Core Vortex

In this investigation, the dynamic-stall vortex is modeled as a thick-core vortex above an infinite plane surface. The inviscid flow due to the thick-core vortex consists of a semicircular vortex, in which the vorticity is proportional to the stream function, surrounded by the irrotational flow due to a circular cylinder with a freestream velocity U_0 (Ref. 24, pp. 534, 535). The thick-core vortex is shown schematically in Fig. 2 in a frame of reference moving with the vortex. Note that dimensional variables are denoted with an asterisk. The inviscid vortex has a velocity V_c relative to the wall due to its self-induced flow. Note that, if placed in a stagnant fluid, that is, $U_0 = 0$, a vortex with negative sign rotation (clockwise) will convect in the negative x direction ($V_c < 0$) due to its self-induced velocity.

As in Refs. 18 and 19, the following parameters are defined to characterize the speed of the vortex in an inviscid flow:

$$\alpha = V_c/U_0 \tag{1a}$$

$$\beta = \alpha/(1-\alpha) \tag{1b}$$

where α is the fractional convection rate of the vortex relative to the freestream velocity and β is the nondimensional wall speed in a frame of reference moving with the vortex. In this reference frame, the freestream velocity becomes $U_0(1-\alpha)$. The case with $\alpha = 0$ ($\beta = 0$) corresponds to a vortex with sufficient self-induced velocity to balance exactly the oncoming flow and to remain stationary relative to the wall, that is, $V_c = 0$. This is considered in more detail by Cassel,[21] Obabko,[22] and Obabko and Cassel.[23] As α is increased from zero to one ($0 < \beta < \infty$), the vortex becomes weaker and/or farther from the wall and is convected downstream ($0 < V_c < U_0$). In the limiting case $\alpha \to 1$ ($\beta \to \infty$), the vortex has zero circulation or is an infinite distance from the wall and, therefore, convects with the freestream velocity, that is, $V_c = U_0$. For $-\infty < \alpha < 0$ ($-1 < \beta < 0$), the vortex is sufficiently strong and/or close to the wall to overcome the oncoming flow and convect upstream relative to the wall ($V_c < 0$). When $1 < \alpha < \infty$ ($-\infty < \beta < -1$), the rotation of the vortex reverses sign, and the vortex convects downstream with a speed greater than the freestream velocity ($V_c > U_0$). The case with $\alpha \to \infty$ ($\beta \to -1$) corresponds to a vortex propagating in a stagnant fluid, that is, $U_0 = 0$. This case was investigated by Walker[25] and Peridier et al.,[17] who considered the unsteady boundary layer induced by a rectilinear vortex above an infinite plane wall.

The normal distance from the surface to the center of the vortex is given by r_0. When r_0 is taken to be the characteristic length and the velocity at infinity $U_0(1-\alpha)$ is taken to be the characteristic velocity, it is shown by Cassel[21] that the nondimensional stream function in cylindrical coordinates in a frame of reference moving with the vortex for the inviscid flow is

$$\psi_0(r,\theta) = \left[r - \frac{1}{r}\left(\frac{e}{r_0}\right)^2 \right] \sin\theta, \qquad r > e/r_0 \tag{2a}$$

$$\psi_0(r,\theta) = \frac{2}{r_0}\frac{J_1(kr_0 r)}{kJ_0(ke)} \sin\theta, \qquad r \le e/r_0 \tag{2b}$$

where the radius of the vortex is taken as e, the base of the natural logarithm. Here, k is a constant chosen such that ke is the first zero of the first-order Bessel function of the first kind. The inviscid stagnation points on the wall are located at $x = \pm 2.0811$, where

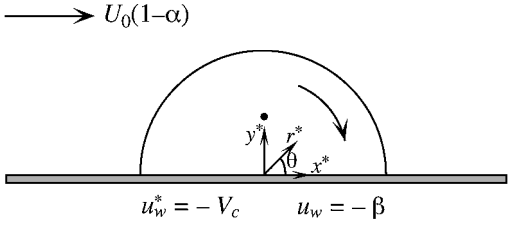

Fig. 2 Schematic of the thick-core vortex in a frame of reference moving with the vortex.

x is the coordinate along the wall, nondimensionalized using r_0, with the origin centered beneath the vortex. Note that kr_0 is the first zero of the derivative of the Bessel function of the first kind. With respect to the local flow direction in the lower portion of the vortex, which is from right to left, the pressure gradient is adverse between the origin and the left stagnation point. Equations (2) prescribe the inviscid solution for the thick-core vortex above an infinite plane wall and provide the initial condition for the impulsively started Navier–Stokes calculations.

B. Solution Methodology

The two-dimensional, incompressible Navier–Stokes equations are solved for the flow induced by the thick-core vortex using the vorticity-stream function formulation. The vorticity-transport equation is

$$\frac{\partial\omega}{\partial t} + u\frac{\partial\omega}{\partial x} + v\frac{\partial\omega}{\partial y} = \frac{1}{Re}\left[\frac{\partial^2\omega}{\partial x^2} + \frac{\partial^2\omega}{\partial y^2}\right] \tag{3}$$

and the Poisson equation for the stream function is

$$\frac{\partial^2\psi}{\partial x^2} + \frac{\partial^2\psi}{\partial y^2} = -\omega \tag{4}$$

The Reynolds number is defined by $Re = U_0(1-\alpha)r_0/\nu$.

A grid transformation is used to focus grid points near the wall and in the streamwise region where unsteady separation occurs; it is given by

$$\hat{x} = (2/\pi)\arctan[(x - x_0)/a] \tag{5a}$$

$$\hat{y} = (2/\pi)\arctan(y/b) \tag{5b}$$

The grid parameters a and b determine the degree of focusing of the grid near x_0, the center of the streamwise transformation, and the wall, respectively. After the flow is impulsively started from the inviscid solution at $t = 0$, the vorticity-transportequation (3) is solved using a factored alternating-direction-implicit (ADI) algorithm with upwind–downwind differencing similar to that of Peridier et al.,[17] and the Poisson equation for stream function (4) is solved using a multigrid algorithm. The multigrid algorithm is $\mathcal{O}(\Delta x^2, \Delta y^2)$ accurate, and the factored-ADI algorithm is $\mathcal{O}(\Delta x\Delta t, \Delta y\Delta t)$ accurate. For additional details concerning the formulation and the numerical techniques used in this investigation, see Cassel,[21] Obabko,[22] and Obabko and Cassel.[23]

III. Results

Navier–Stokes solutions for the flow induced by a thick-core vortex have been obtained in the range from $Re = 10^3$ to 10^5 for $-1.0 \le \beta < \beta_m$, where $\beta_m = |U_e|_{\max} = 2.4829$. Note that the Reynolds number defined here is local, with the characteristic length scale being the height of the vortex above the wall, and would be much higher if based on a global length scale, such as the chord length of an airfoil. The computational grid parameters and time steps used to obtain the results are shown in Table 1. To ensure that all solutions are grid independent, grids with up to four times as many points in the streamwise direction and two times as many points in the normal direction have been used along with time steps as small as 2×10^{-6}.

Detailed results for the case with $\beta = 0$ are described by Cassel,[21] Obabko,[22] and Obabko and Cassel.[23] For the purposes of this investigation, these results for $\beta = 0$ will be viewed as the reference case. This choice is somewhat arbitrary because it simply represents the case for which the inviscid thick-core vortex has sufficient strength such that its self-induced velocity exactly matches the freestream velocity and it does not move relative to the wall. Recall that positive β corresponds to a vortex traveling downstream in the direction of the freestream flow, in which case the wall moves in the negative x direction in a frame of reference moving with the vortex (the same direction as the local inviscid flow in the lower portion of the thick-core vortex). The cases with $-1.0 \le \beta < 0$ correspond to a vortex having sufficient strength to overcome the oncoming flow and travel upstream. In this case, the wall moves in the positive x direction in the vortex frame, which is in the opposite direction to the near-wall flow beneath the vortex.

Table 1 Computational parameters

Re	β/β_m	Grid	a	b	x_0	$\Delta x_{\min}$	$\Delta y_{\min}$	Δt
10^3	0.00	513×513	0.80	0.50	−1.00	4.9×10^{-3}	1.5×10^{-3}	5×10^{-4}
10^4	0.00	1025×513	0.40	0.15	−0.78	1.2×10^{-3}	4.6×10^{-4}	2×10^{-5}
10^4	0.15	513×513	0.80	0.15	−0.90	4.9×10^{-3}	4.6×10^{-4}	5×10^{-4}
10^4	0.25	513×513	0.30	0.15	−0.95	1.8×10^{-3}	4.6×10^{-4}	5×10^{-4}
10^4	0.60	513×513	0.80	0.15	−1.10	4.9×10^{-3}	4.6×10^{-4}	5×10^{-4}
10^4	0.80	513×513	0.80	0.15	−1.30	4.9×10^{-3}	4.6×10^{-4}	5×10^{-4}
10^4	−0.15	513×513	0.40	0.15	−0.80	2.5×10^{-3}	4.6×10^{-4}	5×10^{-6}
10^4	−0.40	513×513	0.40	0.15	−0.80	2.5×10^{-3}	4.6×10^{-4}	5×10^{-6}
10^5	0.80	513×513	0.40	0.05	−1.30	2.5×10^{-3}	1.5×10^{-4}	5×10^{-4}

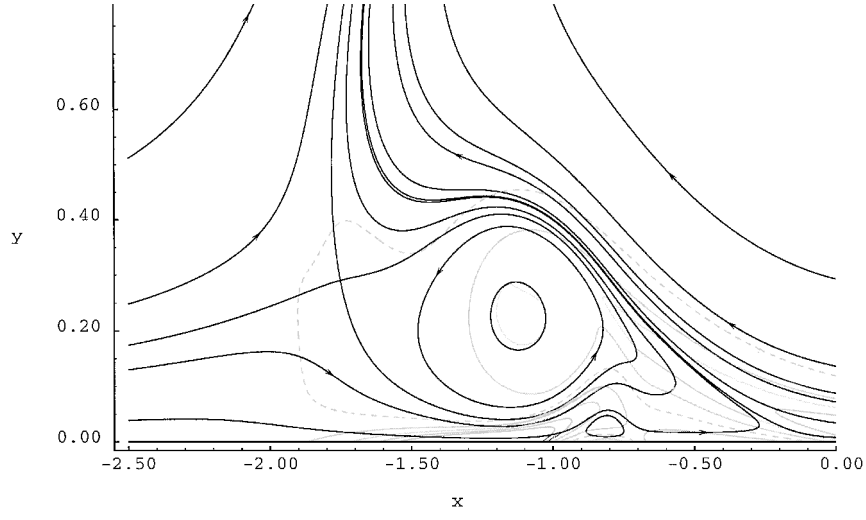

a) $t = 1.9$

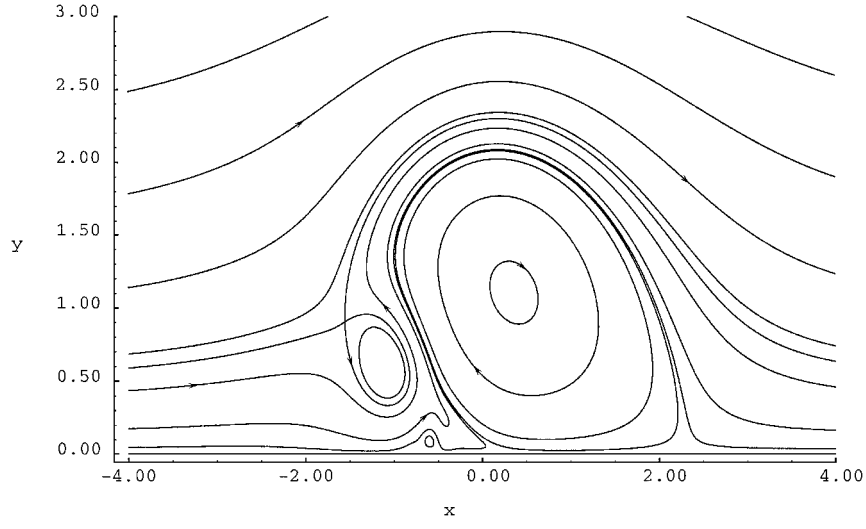

b) $t = 3.0$

Fig. 3 Instantaneous streamlines and vorticity contours for $Re = 10^3$ and $\beta = 0$; – – –, $\omega = 0$.

A. Stationary Wall: $\beta = 0$

To illustrate the typical flow development in the low- and moderate-Reynolds-number regimes discussed in the Introduction, results are shown for $\beta = 0$ at a series of times for $Re = 10^3$, which is representative of the low-Reynolds-number regime, and $Re = 10^4$, representative of the moderate-Reynolds-number regime. Instantaneous streamlines are shown at $t = 1.9$ and $t = 3.0$ for $Re = 10^3$ in Fig. 3. Note that Fig. 3a is a magnified view showing the near-wall flow development, and Fig. 3b is shown on the scale of the thick-core vortex, which is centered at $(x, y) = (0, 1)$ at $t = 0$ (the inviscid solution). In Fig. 3a, the shaded lines are vorticity contours with the dashed line being $\omega = 0$. At $t = 1.9$, the primary recirculation region, which is caused by the adverse pressure gradient induced by the thick-core vortex, is centered near $x = -1.1$. This recirculation region produces its own locally adverse pressure gradient with respect to the near-wall flow direction, which leads to formation of a secondary recirculation region centered near $x = -0.8$. As shown in Fig. 3b, the secondary recirculation region is observed to play a relatively passive role because it has not grown substantially relative to the primary eddy from $t = 1.9$ to 3.0. The primary eddy, which contains vorticity of opposite sign to that of the thick-core vortex, moves away from the surface and interacts with the thick-core vortex, which causes it to move vertically away from the surface and convect downstream. This detachment of the thick-core vortex can

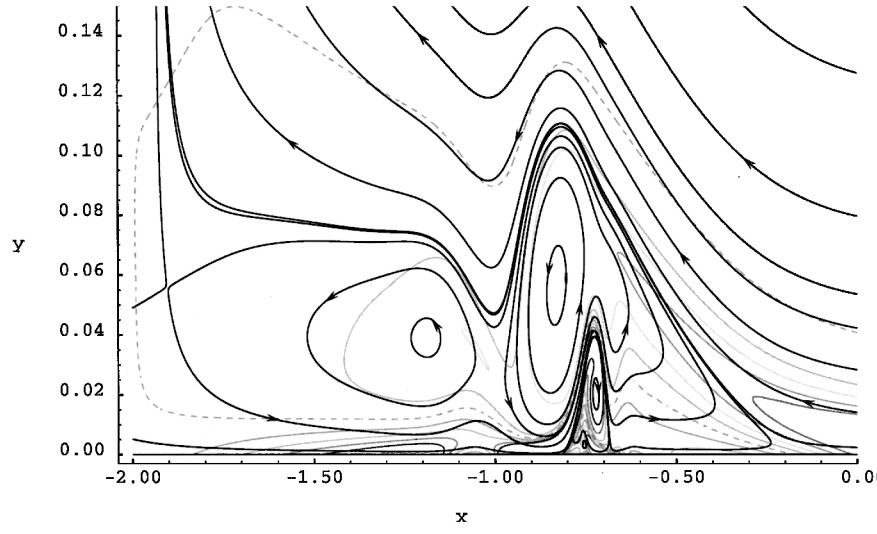

a) $t = 1.55$

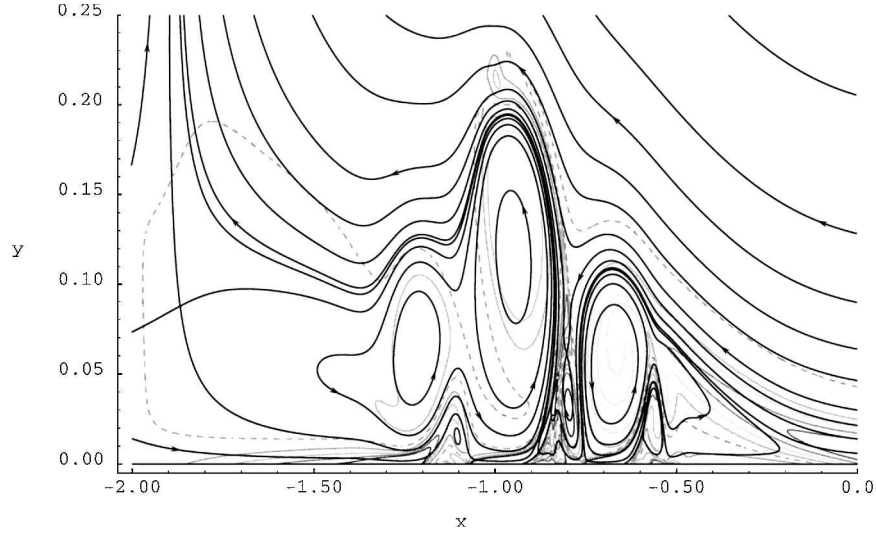

b) $t = 1.9$

Fig. 4 Instantaneous streamlines and vorticity contours for $Re = 10^4$ and $\beta = 0$; – – –, $\omega = 0$.

be observed in Fig. 3b by comparing the streamwise locations of the vortex center and right stagnation point relative to their inviscid locations, $x = 0$ and $x = 2.0811$, respectively.

Results for cases within the moderate-Reynolds-number regime are significantly different in terms of the near-wall flow evolution. Results for $Re = 10^4$ with $\beta = 0$ are shown in Fig. 4 (magnified view) and 5. As shown in Fig. 4a, by $t = 1.55$ a spike has formed near $x = -0.85$, and the primary recirculation region has split into two corotating eddies. For comparison, the noninteracting boundary-layer equations become singular, that is, the spike grows to an infinite distance from the wall on the boundary-layer scale, at $t = 1.402$ for the case with $\beta = 0$ (Ref. 21). In the moderate-Reynolds-number regime, the secondary recirculation region no longer plays a passive role as it does in the low-Reynolds-number regime, instead it expands rapidly away from the surface, splitting the primary recirculation region again near $x = -0.8$, as shown in Fig. 4b. The near-wall vorticity is then ejected away from the surface and wraps around the largest of the primary eddies at $t = 1.9$. At this same time another secondary recirculation region is observed to form near $x = -0.55$ and split the primary eddy again; this process repeats several times on the upstream side of the primary recirculation region. Note that a similar vortex-induced flow was solved numerically by Brinckman and Walker.[26] It was found that an instability appears in the vorticity in regions referred to as alleyways that form between the corotating eddies as observed here. The behavior of this instability in calculations of the thick-core vortex are discussed by Obabko and Cassel.[23]

Results on the scale of the thick-core vortex are shown for later times in Fig. 5. By $t = 2.5$, the two downstream eddies centered near $x = -1.2$ and $x = -0.95$ at $t = 1.9$ (Fig. 4b) have merged to form the largest eddy in Fig. 5a. In a similar fashion, the two downstream eddies then merge again, as shown in Fig. 5b, at $t = 3.0$. This amalgamated eddy then moves away from the surface and interacts with the thick-core vortex, which causes it to detach and convect downstream, as shown in Fig. 5c. Note from a comparison of results at $t = 3.0$ for $Re = 10^3$ (Fig. 3b) and $Re = 10^4$ (Fig. 5b) that the detachment process has advanced further for the lower-Reynolds-number case. Therefore, although the near-wall evolution is much more complex in the moderate-Reynolds-number regime involving formation of a spike, splitting of the primary recirculation region into multiple corotating eddies, ejections of near-wall vorticity and merging of the eddies, the detachment process begins earlier in the low-Reynolds-number regime. In spite of these differences, the detachment process itself appears to be very similar in both the low- and moderate-Reynolds-number regimes. In particular, note the similarity between Fig. 3b and 5c.

Another important difference between the low- and moderate-Reynolds-number regimes may be observed by following the maximum slope of the streamwise pressure gradient along the surface for various Reynolds numbers with $\beta = 0$, as shown in Fig. 6. In Ref. 23, it is explained that the streamwise location of the maximum slope corresponds to the location where the accelerated spike formation occurs in the moderate-Reynolds-number regime

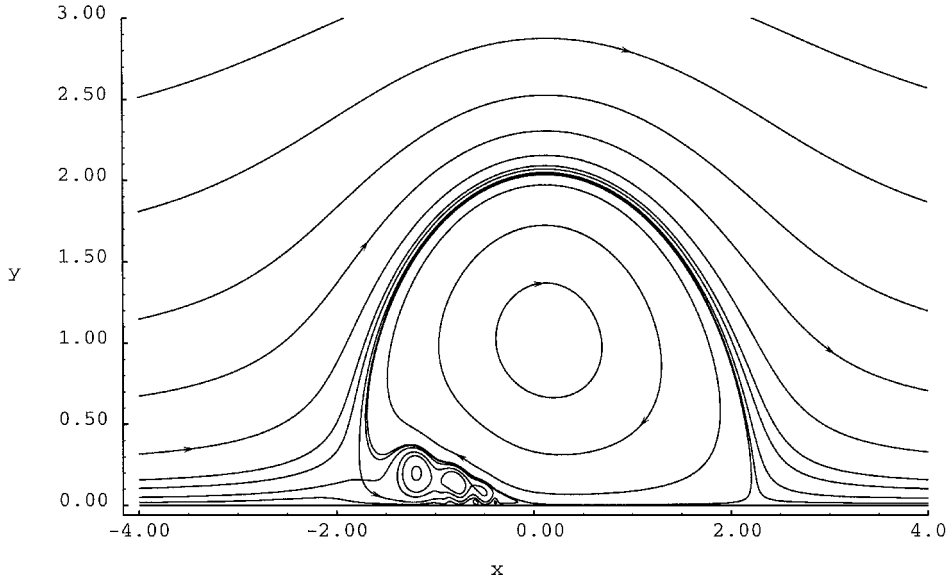

a) $t = 2.5$

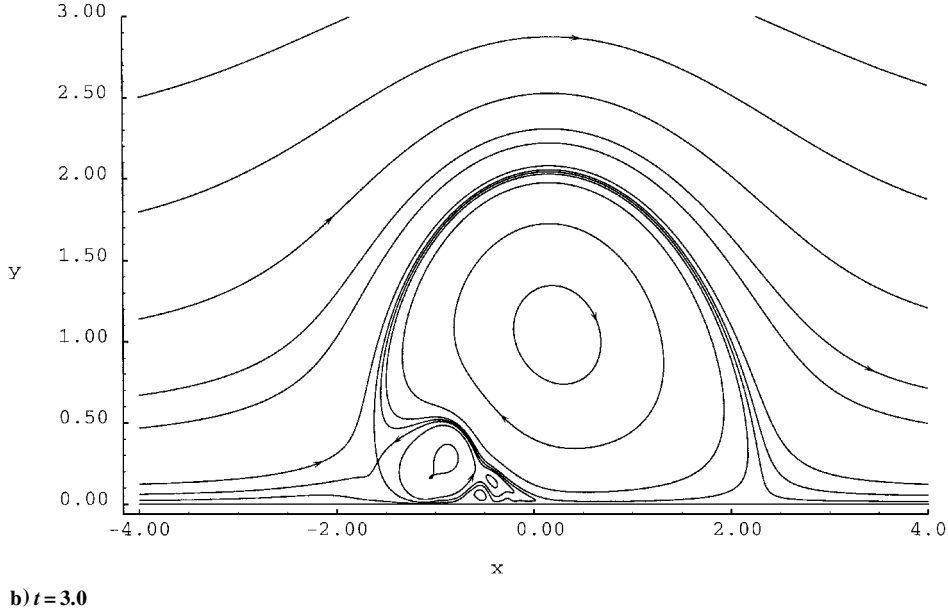

b) $t = 3.0$

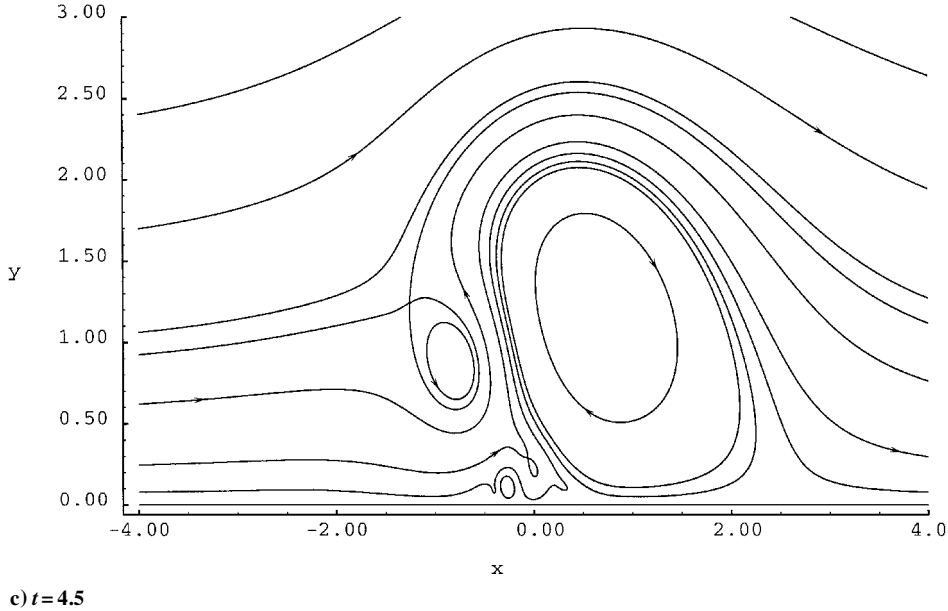

c) $t = 4.5$

Fig. 5 Instantaneous streamlines for $Re = 10^4$ and $\beta = 0$.

due to compression of a portion of the primary recirculation region. For all of the cases except $Re = 10^3$, there is an upstream motion of the spike formation region in the positive x direction over some time interval. This upstream motion contributes to the spike formation process and intensifies as the Reynolds number increases.

B. Moving Wall: $-1.0 \leq \beta < \beta_m$

The influence of a moving wall on these unsteady separation and vortex detachment processes is illustrated through a series of results for $Re = 10^4$ and 10^5 and wall speeds in the range $-1.0 \leq \beta < \beta_m$. Results will be expressed as a percentage of the maximum inviscid wall speed $\beta_m = 2.4829$; the corresponding values of β are given in Table 2. Increasing the wall speed results in a decrease in the difference between the inviscid slip velocity and the wall speed and is expected to lead to a reduction of positive vorticity produced at the wall. A decreasing wall speed, on the other hand, should intensify the initial viscous response of the flow adjacent to the wall and result in higher magnitudes of vorticity of opposite sign to that of the vortex.

Table 2 Wall speed parameters

% of β_m	β
0	0
15	0.3724
25	0.6207
60	1.4897
80	1.9863
100	2.4829

As may be observed from Fig. 7, the influence of wall speed at a fixed Reynolds number has a similar behavior as that for various Reynolds numbers with $\beta = 0$ described in connection with Fig. 6. In particular, there is a range of wall speeds, $\beta \leq 0.15\beta_m = 0.37$, for which there is an upstream motion over some period of time. This upstream motion intensifies with decreasing β, just as with increasing Reynolds number for fixed β, and contributes to the spike formation process. This is illustrated in plots of instantaneous streamlines and vorticity contours at $t = 1.9$ for a series of wall speeds with $Re = 10^4$ in Fig. 8 (cf. Fig. 4b for $\beta = 0$). Whereas the case with $\beta = 0.15\beta_m$ (Fig. 8a) is very similar to that with $\beta = 0$ and indicative of flow in the moderate-Reynolds-number regime, the case with $\beta = 0.6\beta_m$ (Fig. 8b) is similar to that with $Re = 10^3$, $\beta = 0$ (Fig. 3a), which is indicative of the low-Reynolds-number regime. In particular, there is no spike on a scale distinct from the primary recirculation region, and the secondary recirculation region remains passive and does not grow and split the primary recirculation region. As the wall speed is increased further, the primary recirculation region does not form, as shown in Fig. 8c for $\beta = 0.8\beta_m = 1.9863$, and the streamlines and vorticity contours suggest formation of a spike near $x = -1.75$.

Results for the same cases shown in Fig. 8 are shown on the scale of the thick-core vortex in Fig. 9 at a time of $t = 3.0$ to observe the

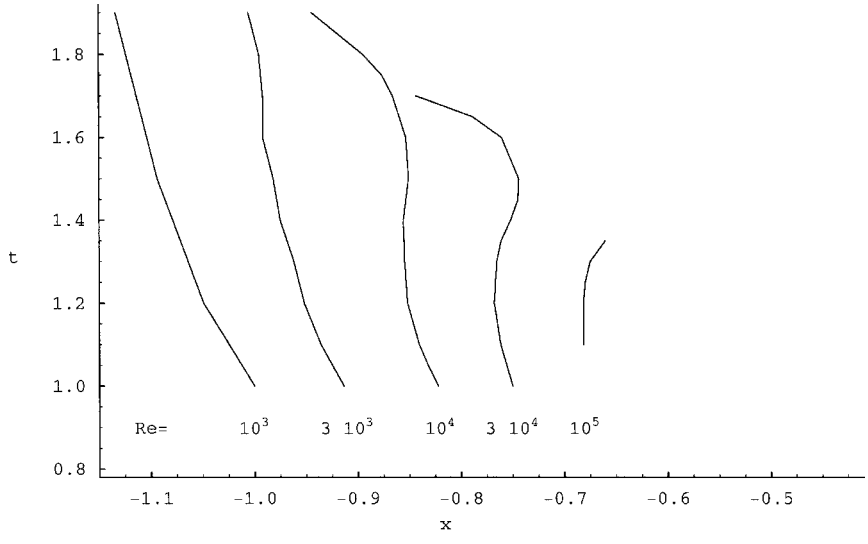

Fig. 6 Location of the maximum slope in streamwise pressure gradient in the spike formation region for various Reynolds numbers with $\beta = 0$.

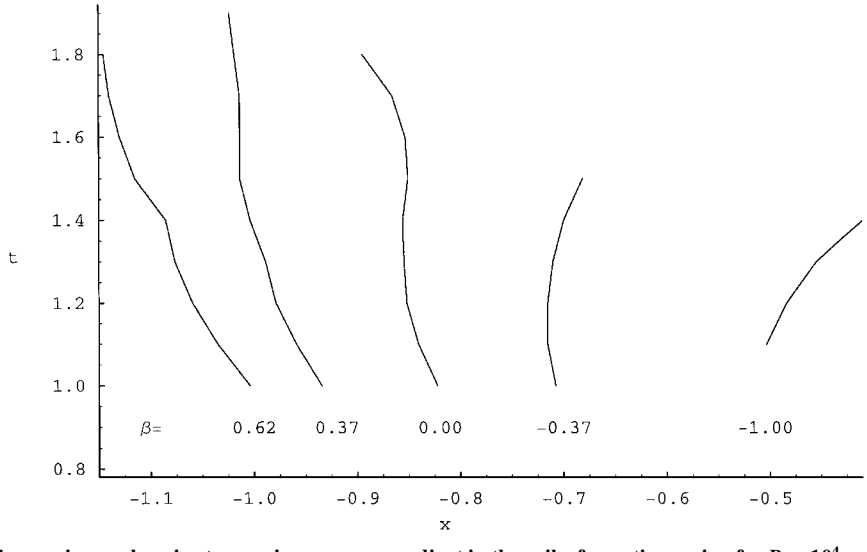

Fig. 7 Location of the maximum slope in streamwise pressure gradient in the spike formation region for $Re = 10^4$ and several wall speeds.

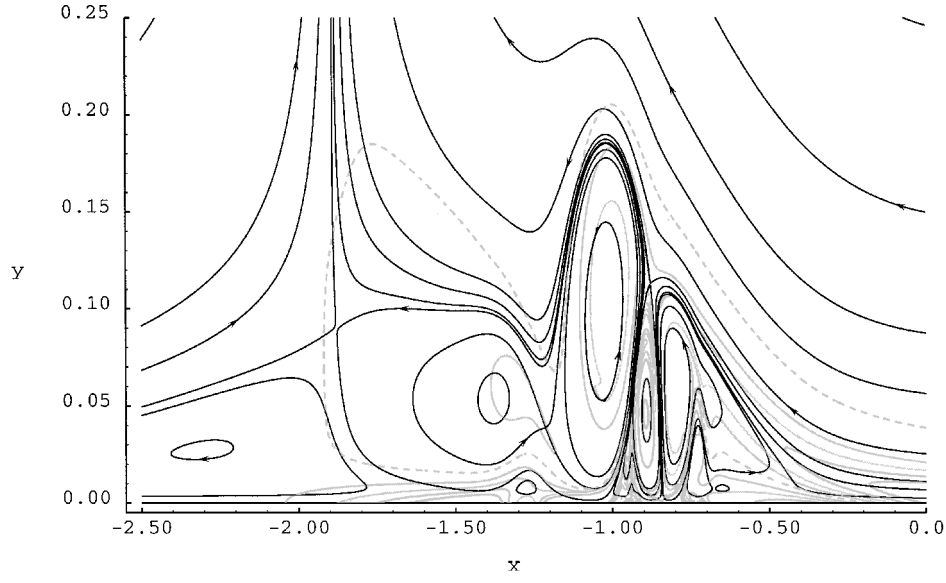

a) $\beta = 0.15\beta_m$

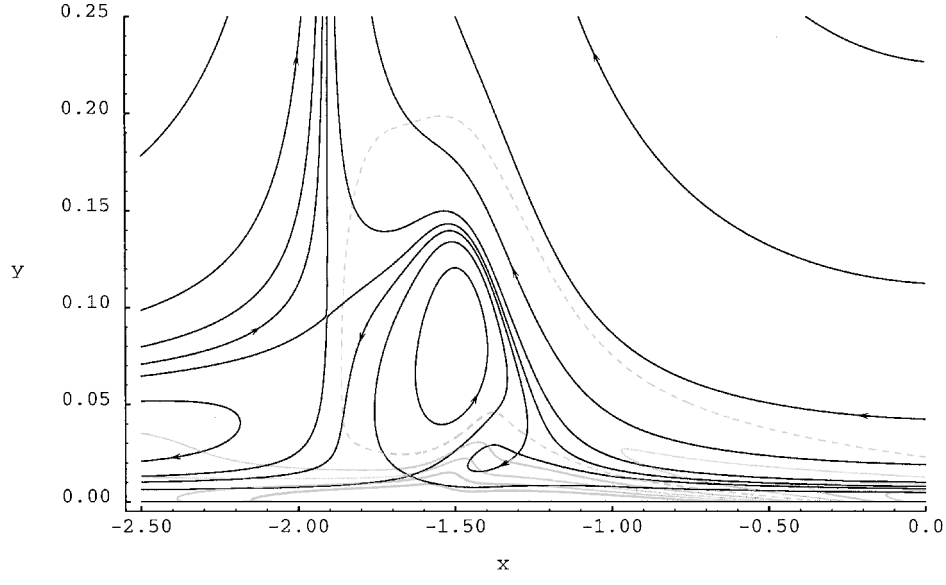

b) $\beta = 0.6\beta_m$

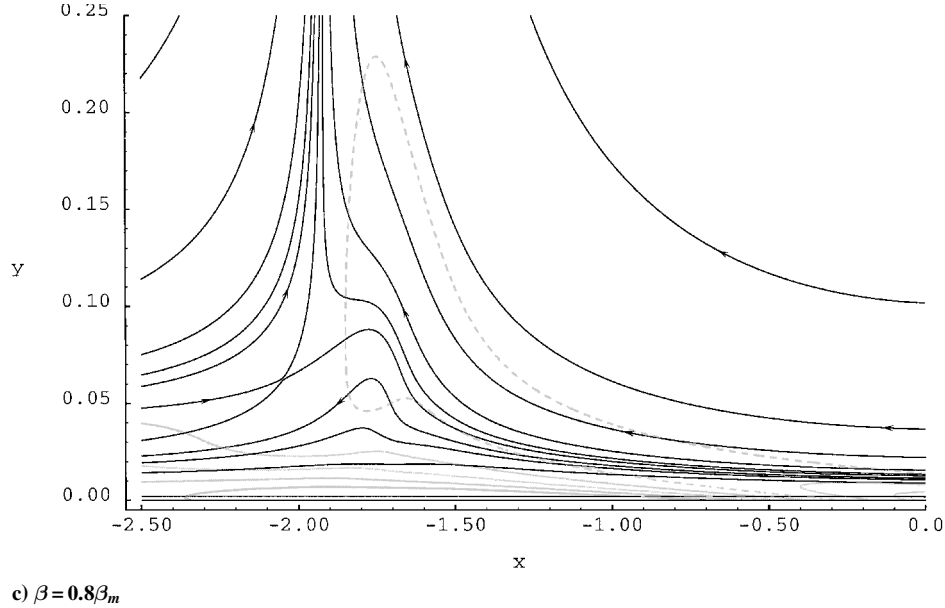

c) $\beta = 0.8\beta_m$

Fig. 8 Instantaneous streamlines and vorticity contours at $t = 1.9$ for $Re = 10^4$ and various wall speeds; – – –, $\omega = 0$.

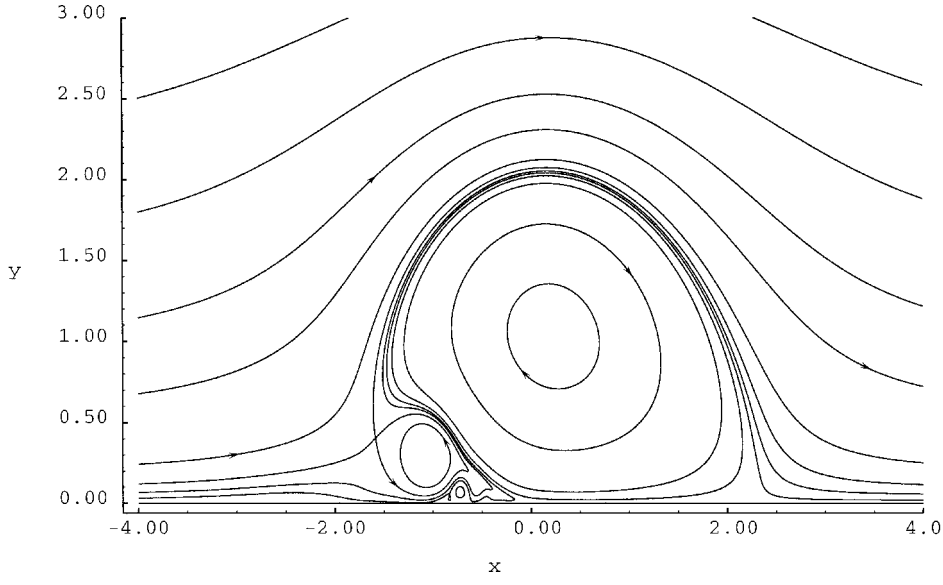

a) $\beta = 0.15\beta_m$

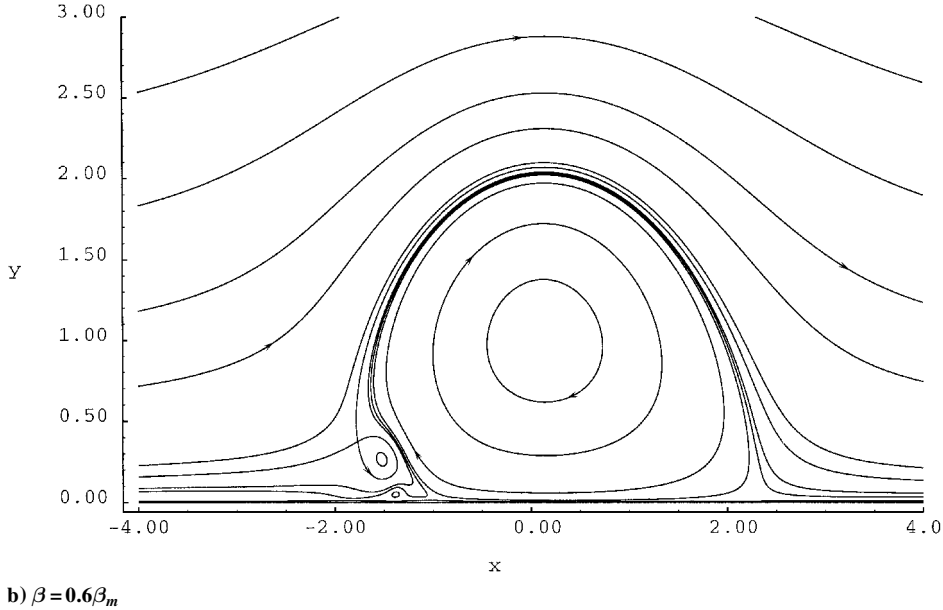

b) $\beta = 0.6\beta_m$

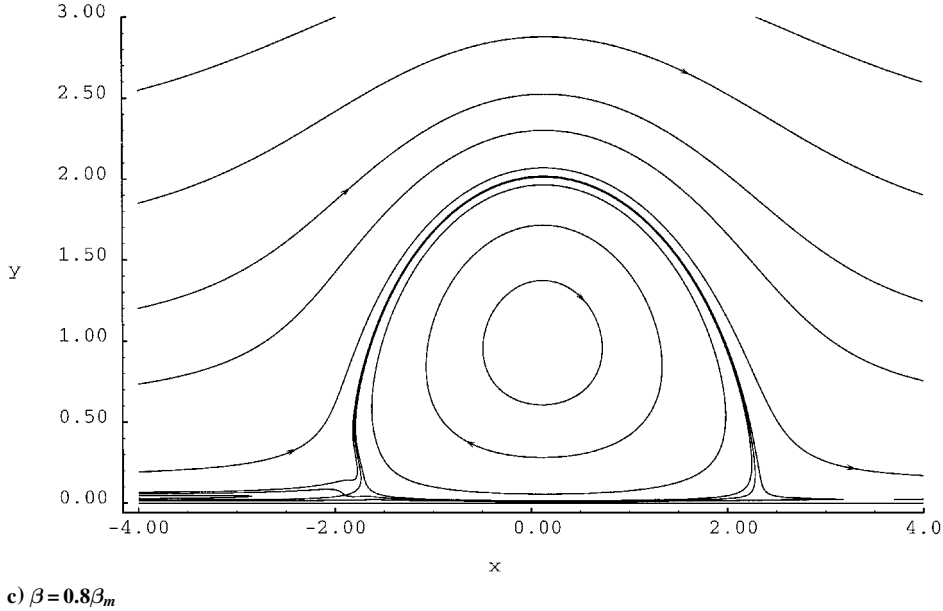

c) $\beta = 0.8\beta_m$

Fig. 9 Instantaneous streamlines at $t = 3.0$ for $Re = 10^4$ and various wall speeds.

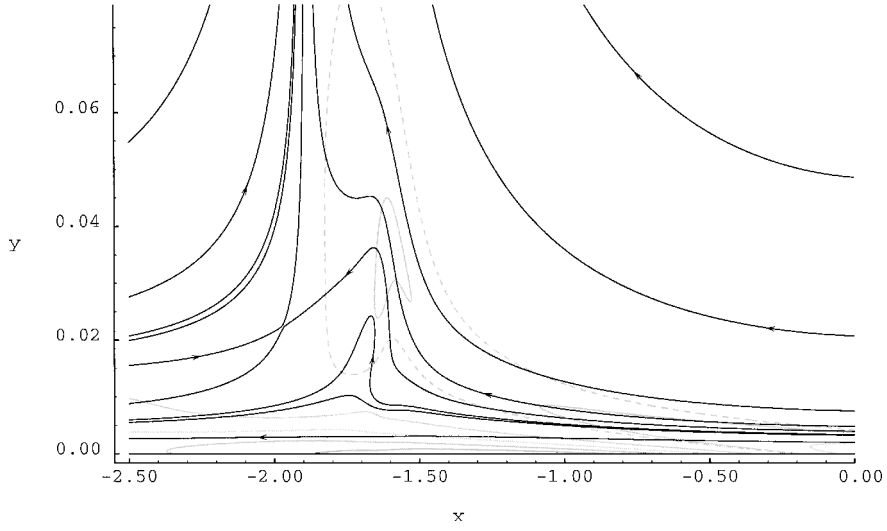

Fig. 10 Instantaneous streamlines and vorticity contours at $t = 1.9$ for $Re = 10^5$ and $\beta = 0.8\beta_m$; – – –, $\omega = 0$.

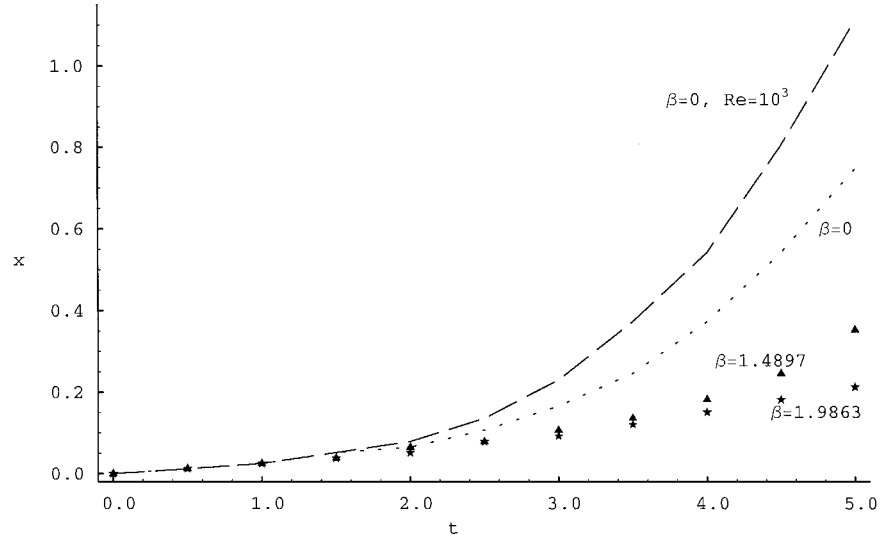

a) Streamwise trajectory

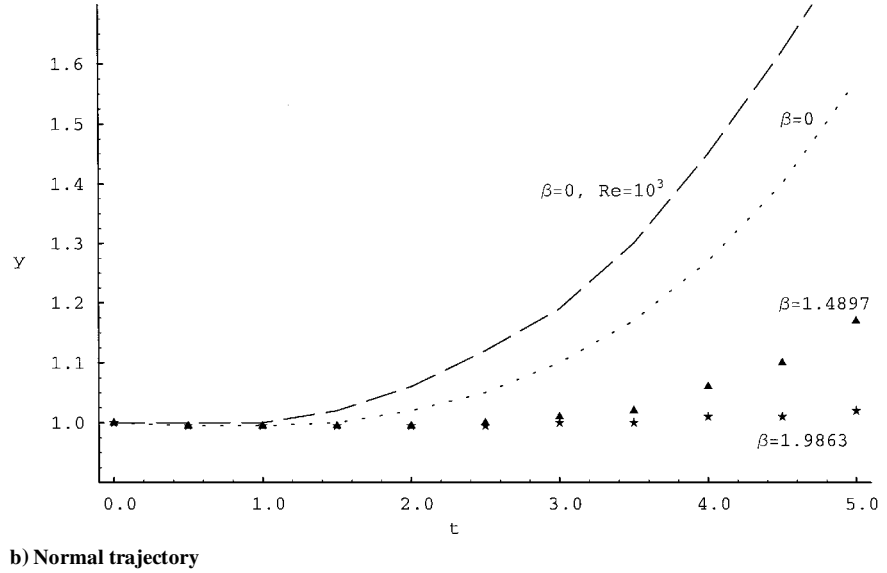

b) Normal trajectory

Fig. 11 Streamwise and normal trajectory of the center of the thick-core vortex for $Re = 10^3$, $\beta = 0$ (– – –) and $Re = 10^4$, $\beta = 0$ (· · · ·), $\beta = 1.4897$ (▲), and $\beta = 1.9863$ (⋆).

influence of the wall speed on the vortex detachment process. These can be compared with Figs. 3b and 5b, which show the results for $Re = 10^3$ and 10^4, respectively, with $\beta = 0$ at this same time. All of the cases in both the low- and moderate-Reynolds-number regimes detach in a very similar fashion; however, this process is delayed somewhat and ultimately suppressed with increasing β. In particular, the results for $\beta \leq 0.6\beta_m \approx 1.5$ are reminiscent of the vortex detachment for the case with $\beta = 0$. For $\beta = 0.8\beta_m \approx 2.0$, however, the streamline behavior resembles the inviscid stream function field at the impulsive start, which indicates that suppression of the primary recirculation region and vortex detachment has occurred.

For comparison with the results for $Re = 10^4$, $\beta = 0.8\beta_m$ at $t = 1.9$ in Fig. 8c, results are shown at the same time and wall speed for a case with $Re = 10^5$ in Fig. 10. The higher Reynolds number results in the streamlines and vorticity contours more abruptly focusing in a region of smaller streamwise extent near $x = -1.65$. A solution of the unsteady boundary-layer equations for $\beta = 2.0$ results in a singularity located at $x_s = -1.57$ at $t_s = 1.81$ (Fig. 1) and also does not exhibit a recirculation region. These Navier–Stokes results for $Re = 10^5$ and $\beta = 0.8\beta_m = 1.9863$ are also very similar to the unsteady boundary-layer results with a moving wall given by Degani et al.[19] for the flow induced by a rectilinear vortex and a rotating cylinder.

The influence of Reynolds number and wall speed on the detachment process is clearly illustrated by tracking the trajectory of the center of the thick-core vortex, determined by tracing the local minimum in vorticity, as shown in Fig. 11. The streamwise and normal trajectory of the center of the thick-core vortex is tracked with time in a frame of reference moving at the inviscid convection velocity of the vortex. Recall that the location of the vortex in the inviscid solution is $(x, y) = (0, 1)$. Note that the slopes of the position curves are the streamwise and normal speeds of the center of the thick-core vortex in this reference frame. For the low- and moderate-Reynolds-number regimes of near-wall flow development, trajectories are shown for $\beta = 0$ with $Re = 10^3$ (dashed lines) and $Re = 10^4$ (dotted lines), respectively. It is evident that both the streamwise and normal speed of the vortex begins increasing earlier for the lower-Reynolds-number case, and the vortex significantly deviates from the initial inviscid location sooner for the flow with the lower Reynolds number. Vortex detachment, therefore, is accompanied by a normal movement away from the surface and a streamwise convection. It is believed that interaction between the thick-core vortex and the separating recirculation region in the low-Reynolds-number regime or the amalgamated eddy in the moderate-Reynolds-number regime leads to the normal movement of the thick-core vortex, effectively weakening it and causing it to detach and convect downstream with the oncoming flow.

To show how increasing the wall speed β suppresses detachment of the thick-core vortex, trajectories are also shown in Fig. 11 for $Re = 10^4$ with $\beta = 0.6\beta_m = 1.4897$ (triangles) and $\beta = 0.8\beta_m = 1.9863$ (stars). Comparison with the trajectories for $\beta = 0$ shows that increasing the wall speed delays an increase in the slopes of the x and y trajectories to later times, which signals a deceleration of the vortex detachment process. Similarly, decreasing the Reynolds number while holding the wall speed constant accelerates the detachment process. In terms of the near-wall flow development, however, both cases have the effect of transitioning the flow from the moderate to the low Reynolds number behavior.

IV. Conclusions

Numerical solutions of the Navier–Stokes equations for the flow induced by a thick-core vortex are given for a range of Reynolds numbers and wall speeds to determine the effect of a moving wall on the unsteady separation and vortex detachment processes. Neglecting viscous effects, the thick-core vortex would remain a constant distance above the wall ($y = 1$ in nondimensional coordinates) and travel with a constant streamwise speed relative to the wall, that is, remain at $x = 0$ in a frame of reference moving with the vortex. When viscous effects are included, a complex sequence of events ensues eventually leading to detachment of the thick-core vortex, after which the vortex convects downstream with the oncoming flow. One would expect this detachment process to be somewhat different in the low- and moderate-Reynolds-number regimes defined by Obabko and Cassel[23] because the former does not involve formation of a rapidly growing spike, whereas the latter does. These results, however, show that, although the unsteady separation process that leads up to detachment is quite different in the low- and moderate-Reynolds-number regimes, the detachment process itself is very similar.

The presence of the vortex induces an adverse pressure gradient that leads to formation of a recirculation region. As this recirculation region grows, its local adverse pressure gradient leads to formation of a secondary recirculation region. In the low-Reynolds-number regime, the primary recirculation region moves away from the surface and interacts with the thick-core vortex, which causes it to detach from the surface. In the moderate-Reynolds-number regime, a spike forms, and a series of secondary recirculation regions appear that ultimately split the primary recirculation region into a series of corotating eddies. These eddies then merge in succession and result in a single amalgamated eddy that then interacts with the thick-core vortex in the same manner as in the low-Reynolds-number regime.

Therefore, that the spike forms in the moderate-Reynolds-number regime, but not in the low-Reynolds-number regime, appears to play a secondary role in terms of the vortex detachment process, at least for the Reynolds numbers considered here. In fact, for cases in the low-Reynolds-number regime, such as $Re = 10^3$ with $\beta = 0$, detachment occurs earlier in nondimensional time than for cases within the moderate-Reynolds-number regime, such as $Re = 10^4$ with $\beta = 0$. Although spike formation is a critical feature in the near-wall flow development, it does not appear to be a good criterion for suppression of vortex detachment for the range of Reynolds numbers considered in this investigation. It is possible that this may change as the Reynolds number is increased and the eruption intensifies. Note that the low-Reynolds-number regime has been considered in this investigation for completeness in understanding the flow for the model problem considered. However, it is likely to have little relevance within the context of dynamic stall as dynamic stall at low Reynolds numbers is significantly influenced by separation propagating upstream from the trailing edge.

A moving wall can have a significant influence on both the unsteady separation and vortex detachment processes. Increasing the wall speed toward the critical value, which is just less than the maximum streamwise velocity of the inviscid flow along the surface $\beta_m = |U_e|_{\max}$, results in suppresssion of the eruptive singularity in calculations of the unsteady boundary-layer equations for $Re \to \infty$ (Ref. 19). Solutions of the Navier–Stokes equations show that this critical wall speed at which spike formation is suppressed decreases with decreasing Reynolds number.[20]

In the present investigation, it is shown that in terms of the near-wall flow development, increasing the wall speed effectively results in behavior that is similar to flows with a fixed wall speed at lower Reynolds numbers. For example, cases that for a particular Reynolds number with $\beta = 0$ are in the moderate-Reynolds-number regime can be transitioned to the low-Reynolds-number regime by increasing the wall speed. The vortex detachment process, however, is delayed with increasing wall speed, until a wall speed close to the maximum inviscid streamwise velocity is reached above which the recirculation region does not form and vortex detachment is suppressed. Therefore, it is not sufficient to only suppress formation of the spike that occurs in the moderate- and high-Reynolds-number regimes. Instead, control of detachment of the dynamic-stall vortex requires elimination of the recirculation region, that is, viewed in a frame of reference moving with the vortex.

Acknowledgments

This work has been supported by the U.S. Army Research Office under Contract DAAG55-98-1-0384, Thomas L. Doligalski, Technical Monitor.

References

[1] McCroskey, W. J., "Unsteady Airfoils," *Annual Review of Fluid Mechanics*, Vol. 14, 1982, pp. 284–311.

[2] Carr, L., "Progress in Analysis and Prediction of Dynamic Stall," *Journal of Aircraft*, Vol. 25, No. 1, 1988, pp. 6–17.

[3] Doligalski, T. L., Smith, C. R., and Walker, J. D. A., "Vortex Interactions with Walls," *Annual Review of Fluid Mechanics*, Vol. 26, 1994, pp. 573–616.

[4]Visbal, M. R., and Shang, J. S., "Investigation of the Flow Structure Around a Rapidly Pitching Airfoil," *AIAA Journal*, Vol. 27, No. 8, 1989, pp. 1044–1051.

[5]Shih, C., Lourenco, L., Van Dommelen, L., and Krothapalli, A., "Unsteady Flow Past an Airfoil Pitching at a Constant Rate," *AIAA Journal*, Vol. 30, No. 5, 1992, pp. 1153–1161.

[6]Ghia, K. N., Yang, J., Osswald, G. A., and Ghia, U., "Physics of Forced Unsteady Flow for a NACA 0015 Airfoil Undergoing Constant-Rate Pitch-Up Motion," *Fluid Dynamics Research*, Vol. 10, 1992, pp. 351–369.

[7]Acharya, M., and Metwally, M. H., "Unsteady Pressure Field and Vorticity Production over a Pitching Airfoil," *AIAA Journal*, Vol. 30, No. 2, 1992, pp. 403–411.

[8]Ghosh Choudhuri, P., Knight, D. D., and Visbal, M. R., "Two-Dimensional Unsteady Leading-Edge Separation on a Pitching Airfoil," *AIAA Journal*, Vol. 32, No. 4, 1994, pp. 673–681.

[9]Ghosh Choudhuri, P., and Knight, D. D., "Effects of Compressibility, Pitch Rate, and Reynolds Number on Unsteady Incipient Leading-Edge Boundary-layer Separation over a Pitching Airfoil," *Journal of Fluid Mechanics*, Vol. 308, 1996, pp. 195–217.

[10]Degani, A. T., Li, Q., and Walker, J. D. A., "Unsteady Separation from the Leading Edge of a Thin Airfoil," *Physics of Fluids*, Vol. 8, No. 3, 1996, pp. 704–714.

[11]Morgan, P. E., and Visbal, M. R., "Simulation of Unsteady Three-Dimensional Separation on a Pitching Wing," AIAA Paper 2001-2709,2001.

[12]Chandrasekhara, M. S., Wilder, M. C., and Carr, L. W., "Control of Flow Separation Using Adaptive Airfoils," AIAA Paper 97-0655, 1997.

[13]Karim, M. A., and Acharya, M., "Suppression of Dynamic-Stall Vortices over Pitching Airfoils by Leading-Edge Suction," *AIAA Journal*, Vol. 32, No. 8, 1994, pp. 1647–1655.

[14]Alrefai, M., and Acharya, M., "Controlled Leading-Edge Suction for Management of Unsteady Separation over Pitching Airfoils," *AIAA Journal*, Vol. 34, No. 11, 1996, pp. 2327–2336.

[15]Cassel, K. W., "The Effect of Convective Heat Transfer on Unsteady Boundary-Layer Separation," *Journal of Fluid Mechanics*, Vol. 428, 2001, pp. 107–131.

[16]Van Dommelen, L. L., "Unsteady Boundary-Layer Separation," Ph.D. Dissertation, Sibley School of Mechanical and Aerospace Engineering, Cornell Univ., Ithaca, NY, May 1981.

[17]Peridier, V. J., Smith, F. T., and Walker, J. D. A., "Vortex-Induced Boundary-Layer Separation. Part 1. The Unsteady Limit Problem $Re \rightarrow \infty$," *Journal of Fluid Mechanics*, Vol. 232, 1991, pp. 99–131.

[18]Doligalski, T. L., and Walker, J. D. A., "The Boundary Layer Induced by a Convected Two-Dimensional Vortex," *Journal of Fluid Mechanics*, Vol. 139, 1984, pp. 1–28.

[19]Degani, A. T., Walker, J. D. A., and Smith, F. T., "Unsteady Separation Past Moving Surfaces," *Journal of Fluid Mechanics*, Vol. 375, 1998, pp. 1–38.

[20]Cassel, K. W., and Obabko, A. V., "The Influence of a Moving Wall on Unsteady Separation," AIAA Paper 99-1005, 1999.

[21]Cassel, K. W., "A Comparison of Navier–Stokes Solutions with the Theoretical Description of Unsteady Separation," *Philosophical Transactions of the Royal Society of London, Series A*, Vol. 358, 2000, pp. 3207–3227.

[22]Obabko, A. V., "Navier–Stokes Solutions of Unsteady Separation Induced by a Vortex—Comparison with Theory and Influence of a Moving Wall," Ph.D. Dissertation, Mechanical, Materials and Aerospace Engineering Dept., Illinois Inst. of Technology, Chicago, Dec. 2001.

[23]Obabko, A. V., and Cassel, K. W., "Navier–Stokes Solutions of Unsteady Separation Induced by a Vortex," *Journal of Fluid Mechanics* (to be published).

[24]Batchelor, G. K., *An Introduction to Fluid Dynamics*, Cambridge Univ. Press, Cambridge, England, UK, 1967.

[25]Walker, J. D. A., "The Boundary Layer Due to a Rectilinear Vortex," *Proceedings of the Royal Society of London, Series A: Mathematical and Physical Sciences*, Vol. 359, 1978, pp. 167–188.

[26]Brinckman, K. W., and Walker, J. D. A., "Instability in a Viscous Flow Driven by Streamwise Vortices," *Journal of Fluid Mechanics*, Vol. 432, 2001, pp. 127–166.

A. Plotkin
Associate Editor